Mathematical Biosciences and Engineering

MBE, 19(12): 13374–13398.
DOI: 10.3934/mbe.2022626
Received: 20 June 2022
Revised: 22 August 2022
Accepted: 25 August 2022
Published: 14 September 2022

http://www.aimspress.com/journal/MBE

Research article

Investigation of the mechanisms and experimental verification of Shao yao gan cao decoction against Sphincter of Oddi Dysfunction via systems pharmacology

Yong-hong Hu[1,†], Xue-ying Wang[2,†], Xi-wen Zhang[3], Jian Chen[4,5,*] and Fu Li[3,*]

[1] Institute of Digestive Disease of Integrated Traditional Chinese and Western Medicine, Shuguang Hospital affiliated to Shanghai University of Traditional Chinese Medicine, Shanghai 201203, China
[2] Department of Preventive Treatment, Shuguang Hospital affiliated with Shanghai University of Traditional Chinese Medicine, Shanghai 201203, China
[3] Department of Pancreaticobiliary Surgery, Shuguang Hospital affiliated with Shanghai University of Traditional Chinese Medicine, Shanghai 201203, China
[4] Department of Vascular Disease, Shanghai TCM-Integrated Hospital, Shanghai University of Traditional Chinese Medicine, Shanghai 200082, China
[5] Institute of Vascular Anomalies, Shanghai Academy of Traditional Chinese Medicine, Shanghai 200082, China

† These two authors contributed equally.

* **Correspondence:** Email: alexandercj@126.com, yclifu17@163.com.

Abstract: This study explored the chemical and pharmacological mechanisms of Shao Yao Gan Cao decoction (SYGC) in the treatment of Sphincter of Oddi Dysfunction (SOD) through ultra-high-performance liquid chromatography coupled with Quadrupole Exactive-Orbitrap high-resolution mass spectrometry (UHPLC-Q Exactive-Orbitrap HR-MS), network pharmacology, transcriptomics, molecular docking and in vivo experiments. First, we identified that SYGC improves SOD in guinea pigs by increased c-kit expression and decreased inflammation infiltration and ring muscle disorders. Then, a total of 649 SOD differential genes were found through RNA sequencing and mainly enriched in complement and coagulation cascades, the B cell receptor signaling pathway and the NF-kappa B signaling pathway. By combining

UHPLC-Q-Orbitrap-HRMS with a network pharmacology study, 111 chemicals and a total of 52 common targets were obtained from SYGC in the treatment of SOD, which is also involved in muscle contraction, the B cell receptor signaling pathway and the complement system. Next, 20 intersecting genes were obtained among the PPI network, MCODE and ClusterOne analysis. Then, the molecular docking results indicated that four active compounds (glycycoumarin, licoflavonol, echinatin and homobutein) and three targets (AURKB, KIF11 and PLG) exerted good binding interactions, which are also related to the B cell receptor signaling pathway and the complement system. Finally, animal experiments were conducted to confirm the SYGC therapy effects on SOD and verify the 22 hub genes using RT-qPCR. This study demonstrates that SYGC confers therapeutic effects against an experimental model of SOD via regulating immune response and inflammation, which provides a basis for future research and clinical applications.

Keywords: Sphincter of Oddi Dysfunction; network pharmacology; molecular docking; UHPLC-Q-orbitrap-HRMS; Shao yao gan cao decoction

1. Introduction

The Oddi sphincter (SO) is a precision smooth muscle device at the junction of the bile duct, pancreas and duodenum. It forms a temporal transitional compound movement (MMC) under the multiple and complex regulations of nerves, humors and local reflexes, which play important roles in controlling bile and pancreatic fluid discharge and preventing reflux [1]. Sphincter of Oddi Dysfunction (SOD) is a group of diseases caused by abnormal diastolic function of SO. It is clinically divided into two types, biliary type and pancreatic type, and the former is common [2]. SOD often has no evidence of organic change, but it will bring long-lasting and unbearable trouble to patients. In severe cases, it can be secondary to liver damage, abnormal trypsin and even acute pancreatitis, seriously endangering the life and health of patients [3]. Therefore, it is of great significance to explore the pathological mechanism and drug treatment of SOD.

Shao Yao Gan Cao Tang (SYGC), sourced from *Shang Han Za Bing Lun* in 210 CE, is made up of 2 traditional Chinese medicines: *Paeoniae radix* and *Glycyrrhizae radix* (1:1), which has been used to treat general muscle pain or tremor in skeletal muscles [4]. The *Paeoniae Radix* can nourish blood and relieve the depressed liver, and *Glycyrrhizae Radix* can strengthen the spleen and Qi [5]. It is reported that SYGC can reduce abdominal pain and muscular cramps [4] and suppress duodenal peristalsis during endoscopic retrograde cholangiopancreatography (ERCP) [6]. Our clinical study has indicated that SYGC had good curative effects on SOD, relieving abdominal pain symptoms, improving liver function and reducing bile excretion time [7]. However, its chemical profile responsible for the therapeutic effects on SOD is still unclear.

Recently, network pharmacology and transcriptomics have been widely used to explore the active components and potential mechanisms of traditional Chinese medicine (TCM) [8,9]. In this study, to enable a full assessment of transcriptomics changes in SOD and to increase our understanding of the SYGC mechanism on SOD, ultra-high-performance liquid chromatography coupled with Quadrupole Exactive-Orbitrap high-resolution mass spectrometry (UHPLC-Q Exactive-Orbitrap HR-MS) was first used to identify chemicals of SYGC. Then, transcriptomics and network pharmacology were applied to uncover the mechanism of SYGC in the treatment of SOD.

Finally, the binding affinities between the active compounds and the key targets were determined via molecular docking. Figure 1 shows the flowchart of the study design. This study provides a basis for the clinical application of SYGC in the treatment of SOD.

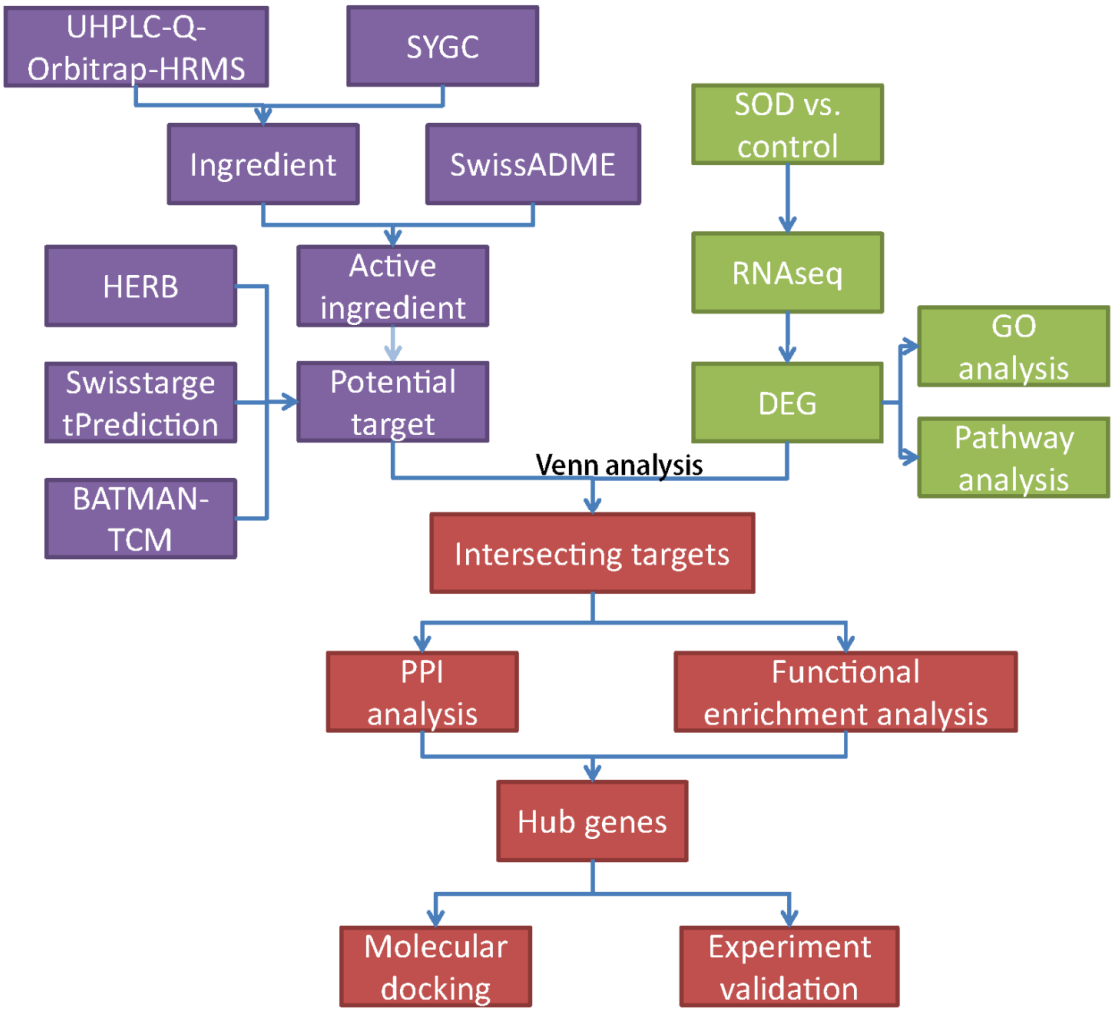

Figure 1. Flowchart of the study design.

2. Materials and methods

2.1. Ultrahigh-performance liquid chromatography quadrupole-Orbitrap high-resolution mass spectrometry (UHPLC-Q-Orbitrap-HR-MS) analysis and identification of target genes of SYGC

The ingredients of SYGC samples were measured by UHPLC-Q-Exactive Orbitrap analysis [10] which was performed by an UHPLC system (UltiMate 3000 RS, Thermo Fisher Scientific, USA) coupled with a Q Exactive Orbitrap (QE, Thermo Fisher Scientific, USA) equipped with an electrospray ionization source (ESI). The protonated molecular weights of all identified compounds were calculated within an error of 10 ppm. Following careful comparisons with the retention times and MS/MS spectra of the reference standards, reference literature, Chemical Book and self-built databases, a total of 111 chemicals were identified or tentatively characterized from SYGC. Then,

active compounds were screened based on the parameters including Lipinski's "rule of five," Ghose #violations and GI absorption, which was performed by a SwissADME (http://www.swissadme.ch/) [11]. The target information of each component of SYGC was obtained from HERB (http://herb.ac.cn/) [12], SwisstargetPrediction (http://swisstargetprediction.ch/) [13] and BATMAN-TCM (http://bionet.ncpsb.org.cn/batman-tcm/index.php/Home/Index/index) [14].

2.2. Establishment of SOD model

The animal experiments were performed by the experimental animal welfare ethics review committee of the Shanghai University of TCM. Forty guinea pigs were purchased from Beijing Vital River Laboratory Animal Technology Co., Ltd. (Beijing, China; qualified production number P2020-052). The guinea pigs were fed under a 12 h cycle of light/dark in IVC conditions and had free access to food and water. The guinea pigs were divided into four groups: control group (N), SOD group (M), SYGC gavage treatment group (G), IRE1 inhibit treatment group (IR) as a positive control group (n = 10/group). The M, G and IR groups were injected intravenously with morphine injection at 0.6 mg/kg body weight, and the normal group was injected intravenously with equal volume of normal saline three times a week for a total of 4 weeks. G group was given orally at 12.5 g/kg per day. The IR group was administered by injection of 30 mg/kg twice a week. After the last administration, all animals were fasted for 12 hours, and the abdominal cavity was opened after anesthesia. After the duodenum was dissected, the white papillary protrusion and the texture of the Oddi sphincter tissue were isolated for follow-up experiments. Blood samples were collected for measurement of alanine aminotransferase (ALT) and aspartate aminotransferase (AST) activities.

2.3. Histological staining

Oddi sphincter tissue samples were fixed in 10% neutral formalin for 48 hours, then dehydrated by conventional gradient, embedded in paraffin, sliced, baked at 60 ℃ for 40 minutes, stained with hematoxylin-eosin (HE) and sealed. The sections were stained with HE to observe the morphological changes such as inflammatory cell infiltration and sphincter injury of Oddi sphincter.

2.4. Total RNA extractions and RNA-Seq analysis

Total RNA in sphincter tissues from the SOD (n = 3) and control samples (n = 3) were extracted using TRIzol Reagent (TIANGEN, China). The purity, concentration and integrity of the total RNA samples were checked for further analysis, and Samples with RNA integrity number (RIN) ≥ 7 were considered to be of high quality. A transcriptome sequencing using the Illumina sequencing platform (HiSeqTM 2500) was conducted on each total RNA sample by OE Biotech Co., Ltd. (Shanghai, China). The raw data were shown in Supplementary data. The differentially expressed genes (DEGs) were screened with $|\log_2$ fold-change (FC)$| \geq 1.0$ and $q \leq 0.05$, which applied for gene ontology (GO) and KEGG enrichment analysis.

2.5. Identification of genes targeted by SYGC in SOD and functional enrichment

To obtain the intersection targets, the key targets of SYGC and SOD DEGs was plotted by

https://www.bioinformatics.com.cn, a free online platform for data analysis and visualization. Metascape platform (https://metascape.org/gp/index.html) [15] was applied to perform Gene ontology (GO) and pathway enrichment analysis (Wiki, Reactome and KEGG pathway) of the above intersection targets.

2.6. Construction of a protein-protein interaction network of the intersecting target genes

The STRING (https://string-db.org/) database was applied to create a protein-protein interaction (PPI) network of intersecting target genes. The Cytoscape 3.9.0 (https://cytoscape. org/) was used to visualize complex relationships between the active chemical components and the target genes. Next, Molecular Complex Detection (MCODE) [16] and ClusterOne analysis [17] were used to find the core targets. MCODE scores ≥ 3 and (node ≥ 3 and $P < 0.05$) were set as the criteria. The number of nodes ≥ 3 and $P < 0.05$ were set as the criteria for ClusterOne analysis.

Table 1. Primer sequence of RT-qPCR.

Gene name	Forward	Reverse
Serpine1	TGGTGGTGACTACTACGACATCCTG	GAATGCTGGTGATGGCGGAGAG
Mmp9	GTGAAGACGCAGACGGTGGATC	TAGAAGCGGTCCTGGCAGAAGTAG
Plg	GTGGCGTTACCTGTCAGAAGTGG	CCTGTTGGTCGTTGTCTGGATTCC
Ccnb1	GTGATGTGGATGCGGAAGATGGAG	GGCTCTCATGTTTCCAGTGACCTC
Cacna2d2	ACTACTCCAATCGCCCCTCT	GAGTAGGAGATGGAGCGTGC
Rad51	TGCGTATGCTCGTGGGTTCAAC	AGCGGTGGCACTGTCTACAATAAG
Prkcb	AAACCATCAAGTGCTCCCTTAACCC	CCCAAATCTCCACGGACAGTCTTC
Alox5	TCACCATCGCCATCAACACCAAG	AGCACAGTGAGGTATAGGTCAGGTC
Adora2a	GCCTATCGCATCCGTGAGTTCC	GTGCCTCCTGCCTTGAAGAGTTC
Chrnb4	GCCGATGGAACCTATGAAGTGTCTG	GGGAAGTGCCTGACCTCAATCTTG
Aurkb	AGAAAGTGGATCTGTGGTGCATTGG	CGCCTGTAAGTCTCGTTGTGTGAG
Top2a	ATGTTGAATGGCACCGAGAAGACC	CGGCTCTCTCCACCTCTGACAG
Tyms	TGCCCTTCAACATTGCCAGCTAC	GTGTGCGTCTCCCAGTGTATGC
Kif11	CGGAAAGCTAACGCCCACTCAG	TCTTATCAGCCAGTCCTCCAGTTCG
Kcnq1	GACGATTGCCTCCTGCTTCTCTG	GCCTCTGCTTCTGCTGGACTTTC
Casq2	ACAACACCAACAATCCTGACCTGAG	GTCTTCTCCCAGTAGGCAACAAGC
Bard1	AGGCAAACAGGGCTCTCAGAAAAC	GAAGGTAGTGGACAAGGCGAATGG
Lck	AGCATAACGGTGAATGGTGGAAGG	CTTGCGGCTCAGGCTCTTGAAG
Jak3	GTGCTGCTCAAGGTGCTGGATG	ACACGAGATGCGGGTAGGACAC
Rasgrp3	CACGCCTCAAAGAGACCCATTCC	TGAAACCATCACAGTCGGCAAAGG
Adipoq	TTTGTGTACCGCTCAGCCTTCAG	GTGGTGCCATCGTAGTGGTTCTG
Gh1	GCTGATGCGGGAACTAGAAGATGG	TCGTTGCTGCGTAAGTTGGTGTC
C-kit	GGCAAGATTTGTGTGTTGTCT	AGATGAAGGGAGAAACTGCTC
Gapdh	CATGTCTGGCAAAGTGGATAT	CGTGGGTAGAATCATACTGGA

2.7. Molecular docking validation

The Protein Data Bank (PDB, https://www.rcsb.org/) was used to obtain the crystal structures of

core targets. The three-dimensional structures of active ingredients were downloaded from PubChem (https://pubchem.ncbi.nlm.nih.gov/). Molecular docking was performed to calculate the binding affinity between active ingredients and core targets by the AutoDock Vina (http://vina.scripps.edu/). The corresponding PDB codes were 4af3, 6hky and 4cik for AURKB, KIF11 and PLG, respectively. We first removed the proteins' water molecules, added polar hydrogen. Then, active pockets were built according to the position of ligand in the PDB complex. The binding energy of ligands in PDB structures was applied for positive control.

2.8. Verifying of hub genes by RT-qPCR

Total RNA was extracted from each sphincter of Oddi tissue using TRIzol (Invitrogen Corporation, CA, USA). cDNA was prepared through cDNA Synthesis SuperMix. Using *Gapdh* as an internal reference, RT-qPCR was performed to detect the mRNA expression levels of intersecting genes among MCODE genes, ClusterONE genes and genes of significant enrichment pathways. The amplification primers were synthesized by Shanghai Sangon Biological Engineering Technology, as shown in Table 1. The mRNA expression level was normalized to that of *Gapdh* in the same sample. The relative expression of each target gene was calculated by the $2^{-\Delta\Delta Ct}$ method.

3. Results

3.1. The effect of SYGC in guinea pig with SOD

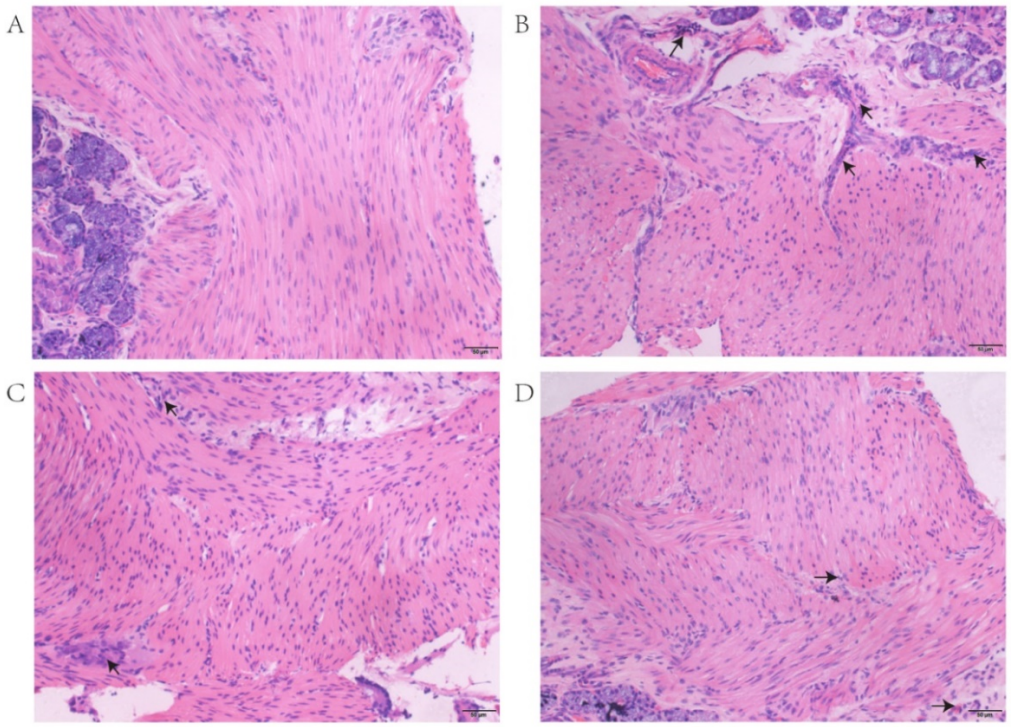

Figure 2. Histomorphology of Oddi sphincter of guinea pigs in each group. A: control group (N), B: SOD group (M), C: SYGC gavage treatment group (G), D: IRE1 inhibit treatment group.

After the model was successfully constructed, the SYGC and positive drug (IRE1 inhibitor) were administered for four weeks. The control group was given the same dose of physiological saline solution. Compared with the normal group, the sphincter tissue of the model group showed edema, increased inflammatory cell infiltration (Figure 2) and decreased c-kit expression (Figure 3), and the ring muscle had partial disorders and irregularities. Also, symptoms such as submucosal fibrous tissue hyperplasia and smooth muscle hypertrophy appeared. After treatment with SYGC or IRE1 inhibitor, the sphincter tissue showed increased c-kit expression and decreased inflammation infiltration, and ring muscle disorders were reduced, suggesting an improved Cajal cell activity in the Oddi sphincter. In addition, compared with the normal group, the serum ALT and AST levels in the model group were significantly higher ($P < 0.01$). Compared with the model group, the serum ALT levels in G and IR group were significantly decreased ($P < 0.01$) (Figure 3), indicating that Shaoyao Gancao Decoction can improve the liver function of SOD guinea pigs.

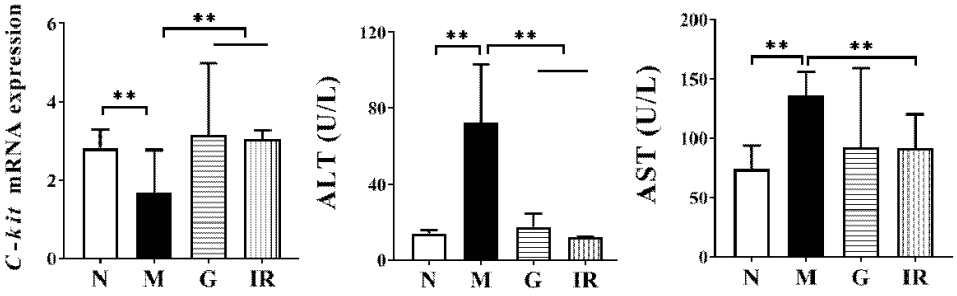

Figure 3. Levels of C-Kit mRNA, ALT and AST expression of guinea pigs in each group. **P < 0.01.

3.2. Identification of compounds and related pharmacological parameters of SYGC

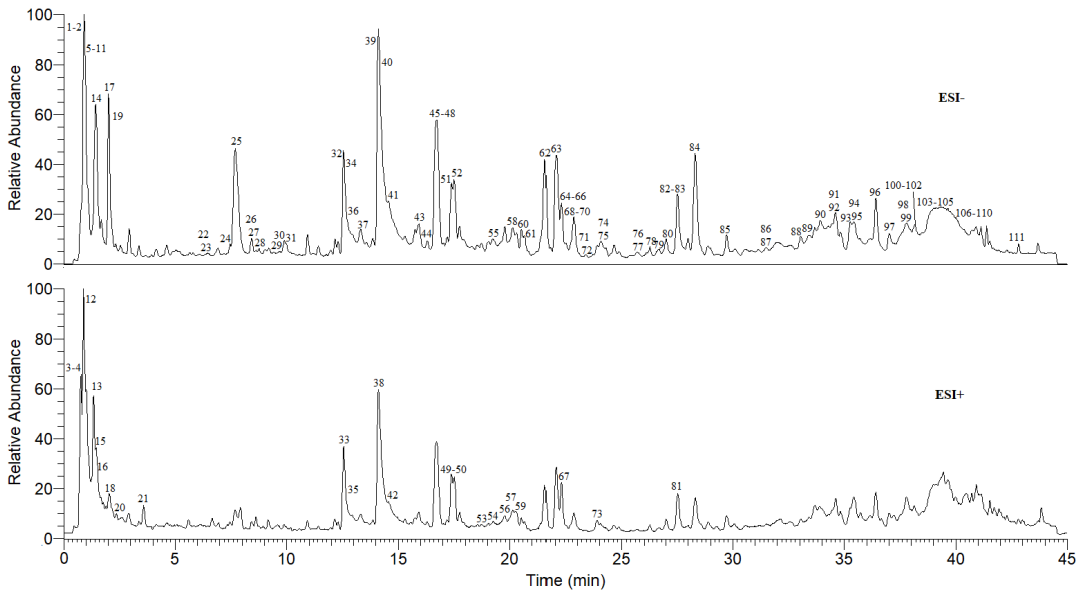

Figure 4. Total ion current diagram of SYGC decoction.

To identify the major chemical components, the SYGC samples were analyzed using the UHPLC-Q-Exactive Orbitrap HR-MS analysis. As shown in Figure 4 and Table 2, 23 compounds were identified under in positive ion mode and 88 compounds were identified under in negative ion mode. Then, Swissadme was applied to explore the pharmacological parameters of these compounds. Finally, 32 candidate compounds passed the parameters (Lipinski's "rule of five," Ghose #violations and GI absorption) and were selected for further research (Table 3). Specifically, 6 ingredients were from *Paeonia lactiflora Pall.*, 22 from *Glycyrrhiza uralensis Fisch.*, and 4 from both herbs.

Table 2. The detailed information of chemical components derived from SYGC by UPLC-Q/TOF-MS.

No.	RT/ min	Ion mode	Measured mass /Da	Calculated mass /Da	Error/ ppm	MS/MS	Molecular formula	Identification	Source
1	0.84	$[M-H]^-$	173.1034	173.1033	0.681	173.10339；156.07675；131.08128	$C_6H_{14}N_4O_2$	Arginine*	M.H.
2	0.88	$[M+FA-H]^-$	195.0501	195.0499	1.030	195.05022；177.03963；129.01799；99.00733	$C_5H_{10}O_5$	Arabinose[x]	M.H.
3	0.89	$[M+H]^+$	118.0867	118.0863	3.598	118.08656；100.07622；72.08146	$C_5H_{11}NO_2$	Valine[x]	M.H.
4	0.89	$[M+H]^+$	138.0551	138.0550	1.267	138.05498；110.06044；94.06567	$C_7H_7NO_2$	Trigonelline[x]	M.H.
5	0.90	$[M-H]^-$	179.0550	179.0550	0.142	179.055	$C_6H_{12}O_6$	Glucose*	M.H.
6	0.90	$[M+FA-H]^-$	549.1670	549.1661	1.547	549.16809；503.16235；341.10956；179.05505	$C_{18}H_{32}O_{16}$	Raffinose[x]	M.H.
7	0.96	$[M-H]^-$	341.1087	341.1078	2.616	341.10913；179.05518；119.03361；89.02291	$C_{12}H_{22}O_{11}$	Sucrose*	M.H.
8	0.98	$[M-H]^-$	191.0552	191.0550	1.023	191.01898；111.00737；87.00727	$C_7H_{12}O_6$	Quinic acid*	M.H.
9	1.01	$[M-H]^-$	149.0080	149.0081	-0.633	149.09593；92.92764	$C_4H_6O_6$	Tartaric acid[x]	M.H.
10	1.09	$[M-H]^-$	133.0128	133.0131	-2.404	133.01285；115.00210；89.02249；71.01216	$C_4H_6O_5$	Malic acid[x]	M.H.
11	1.09	$[M-H]^-$	115.0022	115.0026	-3.175	115.00217；71.01230	$C_4H_4O_4$	Maleic acid[x]	M.H.
12	1.29	$[M+H]^+$	123.0557	123.0553	3.093	123.05553；108.05737；95.08607；80.05014	$C_6H_6N_2O$	Nicotinamide[x]	M.H.
13	1.33	$[M+H]^+$	144.1020	144.1019	0.797	144.10194；100.35320；84.08141	$C_7H_{13}NO_2$	Stachydrine*	GC
14	1.42	$[M-H]^-$	191.0187	191.0186	0.581	191.01889；173.00797；111.00725；87.00718	$C_6H_8O_7$	Citric acid[x]	M.H.
15	1.46	$[M+H]^+$	130.0501	130.0499	1.848	130.05000；84.04503	$C_5H_7NO_3$	Pyroglutamic acid[x]	M.H.
16	1.58	$[M+H]^+$	182.0814	182.0812	1.374	182.13684；165.05475；136.07573；119.04947	$C_9H_{11}NO_3$	Tyrosine*	M.H.
17	2.01	$[M-H]^-$	169.0131	169.0131	-0.235	169.0133；125.0231	$C_7H_6O_5$	Gallic acid*	M.H.

Continued on next page

No.	RT/ min	Ion mode	Measured mass /Da	Calculated mass /Da	Error/ ppm	MS/MS	Molecular formula	Identification	Source
18	2.08	$[M+H]^+$	152.0569	152.0567	1.273	152.05675；135.03027；110.03525	$C_5H_5N_5O$	Guanine*	M.H.
19	2.09	$[M-H]^-$	282.0843	282.0833	3.527	282.08444；150.04097；133.01430；108.01913	$C_{10}H_{13}N_5O_5$	Guanosine*	M.H.
20	2.13	$[M+H]^+$	166.1229	166.1226	1.681	166.12270；149.09624；121.10149；93.07048	$C_{10}H_{15}NO$	Hordenine[x]	GC
21	3.59	$[M+H]^+$	166.0865	166.0863	1.233	166.0862；148.11176；124.03969；106.06532	$C_9H_{11}NO_2$	L-Phenylalanine*	M.H.
22	6.51	$[M-H]^-$	183.0290	183.0288	0.984	183.02908；168.00549；139.03885；124.01530	$C_8H_8O_5$	Methyl Gallate*	SY
23	6.66	$[M-H]^-$	203.0819	203.0815	1.703	203.08202；159.09161；142.06496；116.04915	$C_{11}H_{12}N_2O_2$	Tryptophan[x]	M.H.
24	7.42	[M-H]-	285.0615	285.0605	3.600	285.06174；152.01036；108.02022	$C_{12}H_{14}O_8$	Uralenneoside[x]	GC
25	7.69	[M-H]-	165.0546	165.0546	-0.307	165.05461；141.78123；121.06437；93.03300	$C_9H_{10}O_3$	Phloretic acid[x]	GC
26	8.40	$[M+FA-H]^-$	389.1455	389.1442	3.229	389.14597；343.14001；181.08600；151.07516	$C_{16}H_{24}O_8$	Mudanpioside F[y]	SY
27	8.44	$[M-H]^-$	289.0718	289.0707	3.755	289.07199；245.08183；203.07066；109.02801	$C_{15}H_{14}O_6$	(+)-Catechin*	SY
28	8.73	$[M-H]^-$	121.0281	121.0284	-2.280	121.02818；119.04868；94.02834	$C_7H_6O_2$	4-Hydroxybenzaldehyde[x]	GC
29	9.64	$[M-H]^-$	179.0340	179.0339	0.362	179.03398；135.04384；107.04886	$C_9H_8O_4$	Caffeic acid*	M.H.
30	9.70	$[M-H]^-$	543.1178	543.1167	2.057	543.15491；255.06639；135.00732；119.04897	$C_{23}H_{28}O_{13}S$	Paeoniflorin Sulfite[y]	SY
31	9.88	$[M-H]^-$	495.1507	495.1497	2.014	495.15140；281.06665；137.02313；93.03300	$C_{23}H_{28}O_{12}$	Oxypaeoniflorin*	SY
32	12.53	$[M-H]^-$	121.0279	121.0284	-4.511	121.02815；119.04897；93.03310	$C_7H_6O_2$	3-Hydroxybenzaldehyde*	SY
33	12.54	$[M+H]^+$	197.0810	197.0808	0.632	197.08055；179.07030；133.06485；105.07025	$C_{10}H_{12}O_4$	Paeonilactone B[y]	SY
34	12.55	$[M+FA-H]^-$	525.1610	525.1603	1.414	525.16180；479.15598；283.08264；121.02814	$C_{23}H_{28}O_{11}$	Albiflorin*	SY
35	12.74	$[M+H]^+$	319.1180	319.1176	1.050	319.11862；197.08090；151.07539；105.03388	$C_{17}H_{18}O_6$	Paeoniflorigenone*	SY
36	12.87	[M-H]-	163.0389	163.0390	-0.678	163.03896；119.04886	$C_9H_8O_3$	p-Coumaric acid[x]	M.H.
37	13.01	$[M-H]^-$	197.0447	197.0445	1.219	197.04483；182.02116；166.99760；123.00723	$C_9H_{10}O_5$	Ethyl Gallate*	SY

Continued on next page

No.	RT/ min	Ion mode	Measured mass /Da	Calculated mass /Da	Error/ ppm	MS/MS	Molecular formula	Identification	Source
38	14.02	$[M+H]^+$	195.0654	195.0652	1.306	195.06525；180.04169；135.04424	$C_{10}H_{10}O_4$	Ferulic acid*	SY
39	14.10	$[M+FA-H]^-$	525.1611	525.1603	1.529	525.16205；449.14566；327.10876；121.02717	$C_{23}H_{28}O_{11}$	Paeoniflorin*	SY
40	14.12	$[M-H]^-$	121.0272	121.0284	-9.964	121.02805；119.04849；93.03285	$C_7H_6O_2$	2-Hydroxybenzaldehyde	SY
41	14.58	$[M-H]^-$	593.1513	593.1501	2.046	593.15198；473.10907；383.07767；353.06711	$C_{27}H_{30}O_{15}$	Vcenin-II[x]	GC
42	14.88	$[M+H]^+$	179.0341	179.0339	1.367	179.07022；151.07547；133.06494；105.07031	$C_9H_6O_4$	5,7-Dihydroxycoumarin[x]	GC
43	15.89	$[M-H]^-$	417.1193	417.1180	3.072	417.11948；255.06616；153.01817；119.04880	$C_{21}H_{22}O_9$	Neoliquiritin*	GC
44	16.29	$[M-H]^-$	563.1405	563.1395	1.719	563.14099；443.09879；383.07742；353.06689	$C_{26}H_{28}O_{14}$	Schaftoside[x]	GC
45	16.58	$[M-H]^-$	137.0231	137.0233	-1.683	137.0232； 93.0332	$C_7H_6O_3$	3,4-Dihydroxybenzaldehyde*	M.H.
46	16.60	$[M-H]^-$	563.1405	549.1603	1.719	549.16174；429.10385；255.06619； 135.00745	$C_{26}H_{30}O_{13}$	Naringenin 7-*O*-(2-β-D-Apiofuranosyl)-β-D-glucopyranoside[x]	GC
47	16.64	$[M-H]^-$	563.1404	563.1395	1.613	563.14105；473.10779；383.07770；353.06702	$C_{26}H_{28}O_{14}$	Isoschaftoside[x]	GC
48	16.73	$[M-H]^-$	417.1190	417.1180	2.281	417.11957；255.06628；153.01817；135.00742	$C_{21}H_{22}O_9$	Liquiritin*	GC
49	17.03	$[M+H]+$	581.1873	581.1865	1.339	581.18451；419.13376；257.08060；137.02328	$C_{27}H_{32}O_{14}$	Isoliquiritigenin-4,4'-diglucoside[x]	GC
50	17.34	$[M+H]^+$	465.1036	465.1028	1.715	465.11786；333.18991；135.11693；107.08585	$C_{21}H_{20}O_{12}$	Hyperin*	SY
51	17.52	$[M-H]^-$	549.1613	549.1603	1.917	549.16064；255.06677；153.01819；119.04881	$C_{26}H_{30}O_{13}$	Liquiritin apioside[x]	GC
52	17.73	$[M-H]^-$	631.1669	631.1658	1.780	631.16779；491.11960；313.05685；169.01320	$C_{30}H_{32}O_{15}$	Galloylpaeoniflorin*	SY
53	18.82	$[M+H]^+$	465.1037	465.1028	2.102	465.11781；285.07422；153.12750；135.11693	$C_{21}H_{20}O_{12}$	Isoquercitrin*	SY
54	19.21	$[M+H]^+$	301.0709	301.0707	0.749	301.07056；286.04709；167.03397；105.03389	$C_{16}H_{12}O_6$	Pratensein[x]	GC
55	19.24	$[M-H]^-$	433.1140	433.1129	2.440	433.11423；271.06122；151.00252；119.04887	$C_{21}H_{22}O_{10}$	Chalconaringenin 4-O-glucoside[x]	GC
56	19.73	$[M+H]+$	579.1715	579.1708	1.171	579.17090；325.07077；121.02876	$C_{27}H_{30}O_{14}$	Violanthin[x]	GC

Continued on next page

No.	RT/ min	Ion mode	Measured mass /Da	Calculated mass /Da	Error/ ppm	MS/MS	Molecular formula	Identification	Source
57	20.11	$[M+H]^+$	481.1711	481.1704	1.272	481.19099；197.08093；133.06490；105.03391	$C_{23}H_{28}O_{11}$	Mudanpioside I	SY
58	20.14	$[M-H]^-$	301.0716	301.0707	2.974	301.07159；286.04800；191.03429；150.03105	$C_{16}H_{14}O_6$	Hesperetin*	GC
59	20.27	$[M+H]^+$	301.0708	301.0707	0.549	301.07059；167.03403；105.03387	$C_{16}H_{12}O_6$	Rhamnocitrin[x]	GC
60	20.53	$[M+FA-H]^-$	507.1504	507.1497	1.415	507.15225；461.14590；339.10834；177.05472	$C_{23}H_{26}O_{10}$	Lactiflorin*	SY
61	20.68	$[M-H]^-$	431.0982	431.0973	2.173	431.09805；268.03763	$C_{21}H_{20}O_{10}$	kaempferol-3-rhamnoside[x]	GC
62	21.55	$[M-H]^-$	255.0661	255.0652	3.547	255.06625；153.01811；135.00746；119.04885	$C_{15}H_{12}O_4$	Liquiritigenin*	GC
63	22.01	$[M-H]^-$	417.1190	417.1180	2.425	417.11951；255.06613；119.04876	$C_{21}H_{22}O_9$	Isoliquiritin*	GC
64	22.09	$[M-H]^-$	549.1616	549.1603	1.465	549.16174；255.06610；135.00732	$C_{26}H_{30}O_{13}$	Isoliquiritin Apioside[x]	GC
65	22.22	$[M-H]^-$	459.1298	459.1286	2.715	459.13025；255.06625；153.01826；119.04884	$C_{23}H_{24}O_{10}$	6'-Acetyliquiritin[x]	GC
66	22.28	$[M+FA-H]^-$	475.1245	475.1235	2.205	475.12463；267.06631；252.04248	$C_{22}H_{22}O_9$	Ononin*	GC
67	22.31	$[M+H]^+$	563.1763	563.1759	0.733	563.17450；269.08069	$C_{27}H_{30}O_{13}$	Glycyroside[x]	GC
68	22.57	$[M-H]^-$	591.1721	591.1708	2.179	591.17230；549.16211；255.06621；135.00746	$C_{28}H_{32}O_{14}$	Liquiritigenin-4′-*O*-[β-D-3-*O*-acetyl-apiofuranosyl-(1-2)]-β-D-glucopyranoside[x]	GC
69	22.71	$[M-H]^-$	285.0768	285.0758	3.613	285.07687；270.05347；177.01819；150.03105	$C_{16}H_{14}O_5$	Licochalcone B*	GC
70	22.88	$[M-H]^-$	549.1614	549.1603	2.026	549.16180；417.11899；255.06616；153.01814	$C_{26}H_{30}O_{13}$	Licuraside[x]	GC
71	23.19	$[M-H]^-$	263.1290	263.1278	4.501	263.12851；219.13876；104.11462；151.07529	$C_{15}H_{20}O_4$	(+)-Asycisic acid[x]	M.H.
72	23.25	$[M-H]^-$	599.1773	599.1759	2.324	599.17773；281.06717；137.02309；93.03311	$C_{30}H_{32}O_{13}$	Benzoyloxypaeoniflorin*	SY
73	23.90	$[M+H]^+$	255.0653	255.0652	0.489	255.06505；137.02332；85.57477	$C_{15}H_{10}O_4$	Daidzein*	GC
74	24.03	$[M-H]^-$	695.1986	695.1970	2.249	695.19916；531.15088；255.0612；135.00742	$C_{35}H_{36}O_{15}$	Licorice-glycoside B/D1/D2[x]	GC

Continued on next page

No.	RT/ min	Ion mode	Measured mass /Da	Calculated mass /Da	Error/ ppm	MS/MS	Molecular formula	Identification	Source
75	24.08	[M-H]-	299.0559	299.0550	3.095	299.05618；284.03284；199.03935；147.00769	$C_{16}H_{12}O_6$	7,2',4'—Trihydroxy-5-methoxy-3-arylcoumarin[x]	GC
76	25.71	[M-H]-	285.0768	285.0758	3.718	285.07684；270.05359；177.01857；150.03105	$C_{16}H_{14}O_5$	Homobutein[x]	GC
77	25.91	[M+FA-H]-	491.1196	491.1184	2.499	491.12021；329.13995；153.01823；109.02785	$C_{22}H_{22}O_{10}$	Trifolirhizin[x]	GC
78	26.27	[M-H]-	269.0819	269.0808	4.105	269.046	$C_{16}H_{14}O_4$	Echinatin[x]	GC
79	26.60	[M-H]-	725.2094	725.2076	2.398	725.20972；531.15088；255.06610；135.00740	$C_{36}H_{38}O_{16}$	Licorice-glycoside A/C1/C2	GC
80	27.02	[M+FA-H]-	629.1876	629.1865	1.809	629.18817；583.18237；121.02798	$C_{30}H_{32}O_{12}$	Benzoylalbiflorin*	SY
81	27.17	$[M+H]^+$	287.0552	287.0550	0.681	287.05493；151.03905；121.02861	$C_{15}H_{10}O_6$	Kaempferol*	M.H.
82	27.54	[M+FA-H]-	629.1877	629.1865	1.999	629.18726；583.18323；553.17212；121.02816	$C_{30}H_{32}O_{12}$	Benzoylpaeoniflorin*	SY
83	27.54	[M-H]-	301.0716	301.0707	3.173	301.07151；286.04802；191.03429；150.03101	$C_{16}H_{14}O_6$	Tetrahydroxymethoxychalcone[x]	GC
84	28.31	$[M-H]^-$	255.0660	255.0652	3.233	255.06618；153.01802；135.00734；119.04870	$C_{15}H_{12}O_4$	Isoliquiritigenin*	GC
85	29.71	$[M-H]^-$	267.0662	267.0652	3.650	267.06635；252.04263	$C_{16}H_{12}O_4$	Formononetin*	GC
86	31.54	$[M-H]^-$	837.3913	837.3903	1.162	837.39191；775.39111；485.32816；351.05701	$C_{42}H_{62}O_{17}$	Licorice saponin P2[x]	GC
87	31.90	[M-H]-	895.3972	895.3958	1.579	895.39838；628.15387；351.05673；113.02299	$C_{44}H_{64}O_{19}$	Uralsaponin F[x]	GC
88	33.09	$[M-H]^-$	853.3866	853.3852	1.592	853.38739；351.05695；289.05539；113.02303	$C_{42}H_{62}O_{18}$	22-Hydroxy-licorice saponin G2[x]	GC
89	33.46	$[M-H]^-$	819.3817	819.3798	2.377	819.38220；573.36359；351.05740；193.03456	$C_{42}H_{60}O_{16}$	Licorice saponin E2[x]	GC
90	34.04	$[M-H]^-$	879.4027	879.4009	2.068	879.40271；581.34503；351.05740	$C_{44}H_{64}O_{18}$	22-Acetoxyl-glycyrrhizin[x]	GC
91	34.42	$[M-H]^-$	983.4498	983.4482	1.622	983.44983；821.39618；627.35510；351.05698	$C_{48}H_{72}O_{21}$	Licorice saponin A3[x]	GC
92	34.82	[M-H]-	863.4077	863.4060	1.938	863.40833；758.07990；351.05658；193.03439	$C_{44}H_{64}O_{17}$	22β-Acetoxyglycyrrhaldehyde[x]	GC
93	35.27	$[M-H]^-$	353.1030	353.1020	2.932	353.10287；284.03271；125.02303	$C_{20}H_{18}O_6$	Licoisoflavone A[x]	GC

Continued on next page

No.	RT/ min	Ion mode	Measured mass /Da	Calculated mass /Da	Error/ ppm	MS/MS	Molecular formula	Identification	Source
94	35.46	[M-H]-	353.1395	353.1384	3.341	353.13989；173.03392；165.01820；125.02313	$C_{21}H_{22}O_5$	Gancaonin I[x]	GC
95	35.57	[M-H]-	837.3920	837.3903	1.962	837.39221；732.52264；351.05753；193.03474	$C_{42}H_{62}O_{17}$	Licorice saponin Q2[x]	GC
96	36.42	[M-H]-	367.1186	367.1176	2.575	367.11871；309.04059；203.07121	$C_{21}H_{20}O_6$	Glycycoumarin[x]	GC
97	37.02	[M-H]-	353.1031	353.1020	3.187	353.10321；297.04050	$C_{20}H_{18}O_6$	Licoflavonol[x]	GC
98	37.71	[M-H]-	837.3919	837.3903	1.819	837.39270；732.47290；351.05701	$C_{42}H_{62}O_{17}$	Licorice saponin G2[x]	GC
99	37.90	[M-H]-	337.1447	337.1434	3.780	337.10840；282.05301	$C_{21}H_{22}O_4$	Licochalcone A*	GC
100	38.15	[M-H]-	351.0875	351.0863	3.262	351.08752；333.07715；283.09756；177.01840	$C_{20}H_{16}O_6$	Licoisoflavone B[x]	GC
101	38.44	[M-H]-	837.3919	837.3903	1.891	837.39282；607.58362；351.05847；193.03423	$C_{42}H_{62}O_{17}$	Uralsaponin N[x]	GC
102	38.61	[M-H]-	967.4548	967.4533	1.560	967.45569；860.47540；497.11691	$C_{48}H_{72}O_{20}$	Rhaoglycyrrhizin[x]	GC
103	39.22	[M-H]-	821.3973	821.3954	2.274	821.39740；724.18427；589.77423；351.05710	$C_{42}H_{62}O_{16}$	Glycyrrhizic acid*	GC
104	39.22	[M-H]-	823.4035	823.4111	-9.184	823.41315；574.30713；351.05688；113.02302	$C_{42}H_{64}O_{16}$	Uralsaponin C[x]	GC
105	39.64	[M-H]-	821.3972	821.3954	2.201	821.39734；351.05698；193.03477；113.02299	$C_{42}H_{62}O_{16}$	Licorice saponin H2[x]	GC
106	40.54	[M-H]-	807.4181	807.4161	2.406	807.41821；351.05682；193.03471；113.02308	$C_{42}H_{64}O_{15}$	Licoricesaponin B2[x]	GC
107	40.69	[M-H]-	985.4656	985.4639	1.720	985.46442；497.11523；321.08276；113.02301	$C_{48}H_{74}O_{21}$	Yunganoside D1 or Yunganoside G1[x]	GC
108	40.77	[M-H]-	807.4186	807.4161	2.333	807.41840；351.05688；193.03471；113.02303	$C_{42}H_{64}O_{15}$	22-Dehydroxyural saponin[x]	GC
109	40.90	[M-H]-	821.3978	821.3954	2.203	821.39771；351.05685；193.03465；113.02307	$C_{42}H_{62}O_{16}$	Licorice Saponin K2[x]	GC
110	40.96	[M-H]-	823.4038	823.4111	-8.880	823.41223；351.05713；193.03426；113.02285	$C_{42}H_{64}O_{16}$	Licorice Saponin SJ2[x]	GC
111	42.81	[M-H]-	255.2327	255.2319	3.461	255.13889；149.09576；119.04839；93.03307	$C_{16}H_{32}O_2$	Palmitic Acid[x]	M.H.

*Note: * means that the ingredient was confirmed by the reference substance (Supplementary material); [x] means that ingredient was confirmed by the reference literature "*Chinese Journal of Natural Medicines*, **19** (2021), 305–320. https://doi.org/10.1016/S1875-5364(21)60031-6"; [y] means that ingredient was confirmed by the reference literature *"Journal of Chinese Mass Spectrometry Society,* **35** (2014), 269–278. https://doi.org/10.7538/zpxb.2014.35.03.0269*";* SY: *Paeonia lactiflora Pall.*, GC:*Glycyrrhiza uralensis Fisch.*, M.H.:SY and GC.

Table 3. Chemical properties statistics of 32 potential active hub components from SYGC.

Identification	GI absorption	Lipinski # violations	Ghose # violations	MW	Rotatable bonds	H-bond acceptors	H-bond donors	TPSA
Hordenine	High	0	0	165.23	3	2	1	23.47
Methyl Gallate	High	0	0	184.15	2	5	3	86.99
Phloretic acid	High	0	0	166.17	3	3	2	57.53
(+)-Catechin	High	0	0	290.27	1	6	5	110.38
Caffeic acid	High	0	0	180.16	2	4	3	77.76
Paeonilactone B	High	0	0	196.2	0	4	1	63.6
Paeoniflorigenone	High	0	0	318.32	4	6	1	82.06
p-Coumaric acid	High	0	0	164.16	2	3	2	57.53
Ethyl Gallate	High	0	0	198.17	3	5	3	86.99
Ferulic acid	High	0	0	194.18	3	4	2	66.76
Pratensein	High	0	0	300.26	2	6	3	100.13
Hesperetin	High	0	0	302.28	2	6	3	96.22
Rhamnocitrin	High	0	0	300.26	2	6	3	100.13
Liquiritigenin	High	0	0	256.25	1	4	2	66.76
Ononin	High	0	0	430.4	5	9	4	138.82
Licochalcone B	High	0	0	286.28	4	5	3	86.99
Daidzein	High	0	0	254.24	1	4	2	70.67
7,2',4'－Trihydroxy-5-methoxy -3-arylcoumarin	High	0	0	300.26	2	6	3	100.13
Homobutein	High	0	0	286.28	4	5	3	86.99
Trifolirhizin	High	0	0	446.4	3	10	4	136.3
Echinatin	High	0	0	270.28	4	4	2	66.76
Kaempferol	High	0	0	286.24	1	6	4	111.13
Tetrahydroxymethoxy chalcone	High	0	0	302.28	4	6	4	107.22
Isoliquiritigenin	High	0	0	256.25	3	4	3	77.76
Formononetin	High	0	0	270.28	2	4	1	55.76
Licoisoflavone A	High	0	0	354.35	3	6	4	111.13
Gancaonin I	High	0	0	354.4	5	5	2	72.06
Glycycoumarin	High	0	0	368.38	4	6	3	100.13
Licoflavonol	High	0	0	354.35	3	6	4	111.13
Licochalcone A	High	0	0	338.4	6	4	2	66.76
Licoisoflavone B	High	0	0	352.34	1	6	3	100.13
Palmitic Acid	High	1	0	256.42	14	2	1	37.3

3.3. Identification of target genes of SYGC

The target information of 32 active ingredients was obtained from HERB, SwisstargetPrediction and BATMANTCM. Once duplicate genes were deleted, a total of 1023 targets for SYGC were obtained.

3.4. Identification of SOD differential expression genes and functional enrichment analysis

Furthermore, we explored the dysfunctional genes and pathways in guinea pig SOD using RNA-Seq of sphincter tissues from the Control and SOD groups. The RNA from the three replicate samples from the control and SOD groups was sequenced. In all, 16,281 genes were identified (Supplementary data). To determine the differentially expressed genes (DEGs), a q-value < 0.05 was used as the cut-off value for gene expression in the control and SOD groups using DESeq2. As a result, 649 DEGs including 247 up-regulated and 402 down-regulated genes were screened (Figure 5A). The top 10 enriched GO terms in each category as cellular component (CC), molecular function (MF), biological process (BP) and of the identified DEGs are shown in Figure 5B. The GO terms showed that DEGs were mainly related to negative regulation of cell fate commitment, extracellular space, serine-type endopeptidase inhibitor activity, etc. On the other hand, the results of KEGG enrichment analysis showed that the top enriched KEGG terms were, for example, complement and coagulation cascades, B cell receptor signaling pathway, primary immunodeficiency NF-kappa B signaling pathway (Figure 5C).

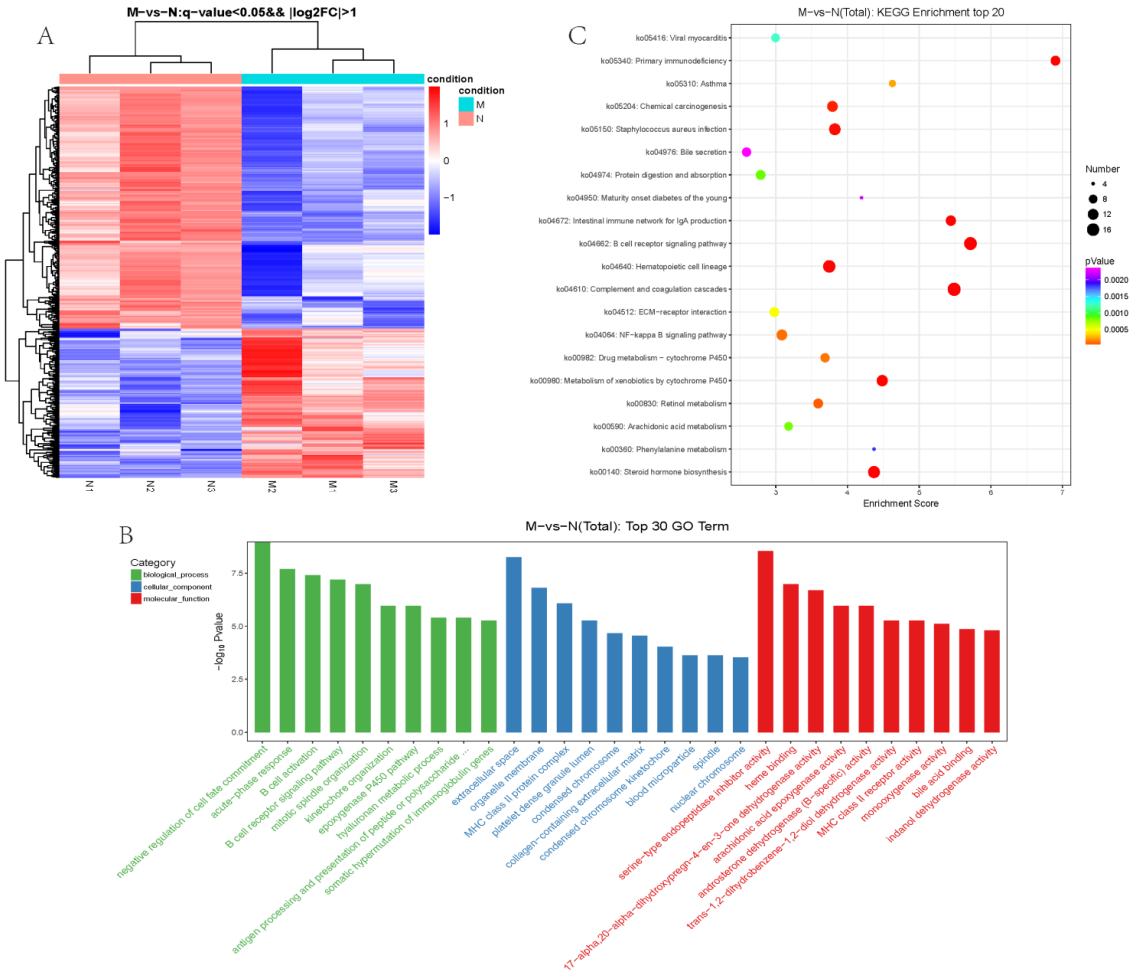

Figure 5. Identification and functional enrichment analyses of DEGs. A: Heatmap of the up- and down-regulated DEGs. B: The top 30 enriched GO terms for DEGs in biological process, molecular function and cellular component categories. C: The top 20 enriched KEGG pathways for DEGs. N: control group, M: SOD group.

3.5. Determination of SOD-related genes targeted by SYGC and functional enrichment analysis

To identify the intersecting genes between SYGC and SOD, a Venn analysis was performed on the target genes of SYGC and SOD DEGs. As shown in Figure 6A, 52 genes were identified as intersecting genes of SYGC and SOD. Then, these intersecting genes were imported into the Metascape database to carry out GO enrichment analysis and pathway enrichment analysis (Figure 6B). BP terms were mainly found in regulation of ion transport, response to xenobiotic stimulus and leukocyte migration. CC terms were mainly enriched in ion channel complex, side of membrane, and perinuclear region of cytoplasm. MF terms were mainly present in kinase binding, kinase binding-membrane spanning protein tyrosine kinase activity and carbonate dehydratase activity. These factors can exert therapeutic effects on SOD.

In addition, the results of the pathway enrichment analysis mainly involved the B cell receptor signaling pathway, complement system, signaling by receptor tyrosine kinases, Interleukin-4 and Interleukin-13 signaling, as well as muscle contraction, among others (Figure 6C).

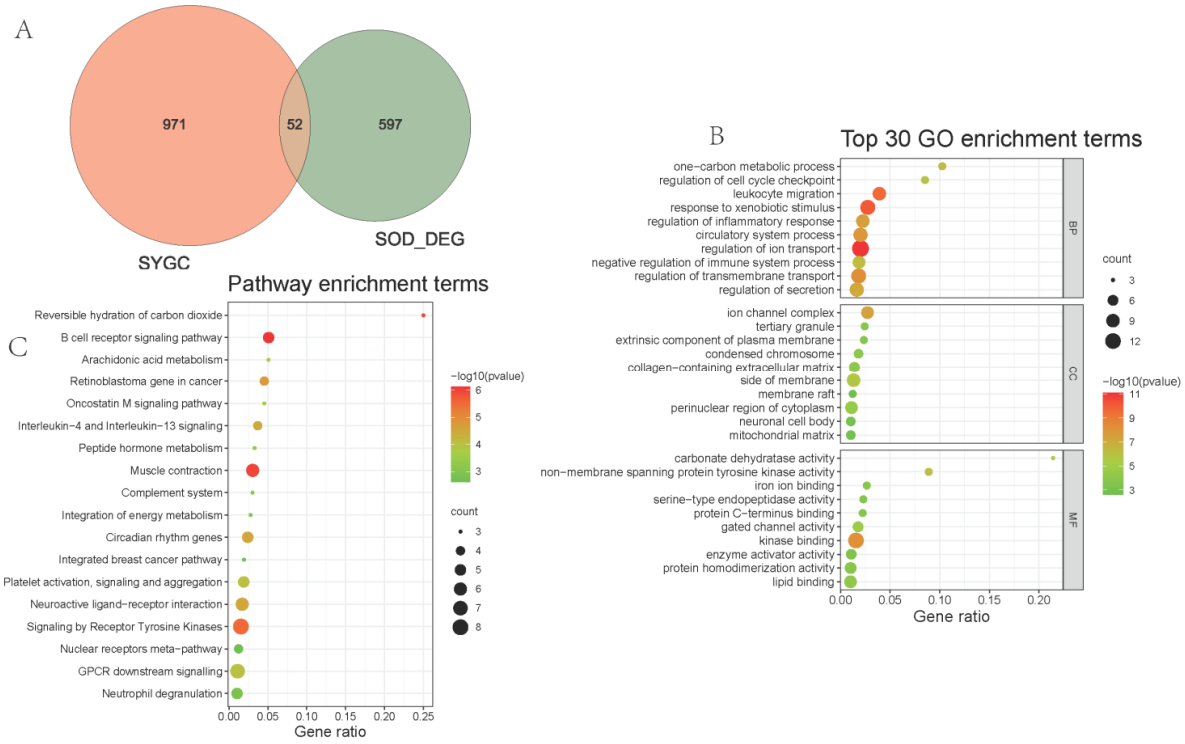

Figure 6. GO and KEGG pathway enrichment analysis of intersecting targets between SYGC and SOD DEGs. A: Venn diagram of the predicted targets of SYGC in SOD. B: The top 30 enriched GO terms for intersecting targets in biological process, molecular function and cellular component categories. C: Enriched KEGG pathways for intersecting targets.

3.6. Analysis of protein-protein interaction network of gene intersection and construction of a regulatory network of targets for the treatment of SOD with SYGC

The STRING database (http://www.string-db.org) was used to investigate the target genes'

interactions. There were 57 nodes and 158 edges in the protein-protein interaction network. Then, the complex interactions between active components and potential target genes were visualized using the Cytoscape, including 82 nodes and 214 edges (Figure 7A). Four significant clusters were obtained from ClusterONE analysis (node ≥ 3 and P < 0.05). Cluster 1 consisted of 10 nodes (Figure 7B); Cluster 2 consisted of 11 nodes (Figure 7C); Cluster 3 consisted of 8 nodes (Figure 7D); Cluster 4 consisted of 3 nodes (Figure 7E). Four significant modules were obtained from MCODE analysis (score ≥ 3). Module 1 (score: 8.75) consisted of 9 nodes (Figure 7F); Module 2 (score: 7.125) consisted of 17 nodes (Figure 7G); module 3 (score: 3.6) consisted of 6 nodes (Figure 7H); module 4 (score: 3) consisted of 3 nodes (Figure 7I). Finally, 20 intersecting genes between MCODE genes and ClusterONE genes were obtained, including SERPINE1, MMP9, PLG, CCNB1, CACNA2D2, RAD51, CHRNB4, AURKB, TOP2A, TYMS, KIF11, KCNQ1, CASQ2, BARD1, CHRNA4, IGFBP1, TNNT2, SCN4A, MKI67, CMA1.

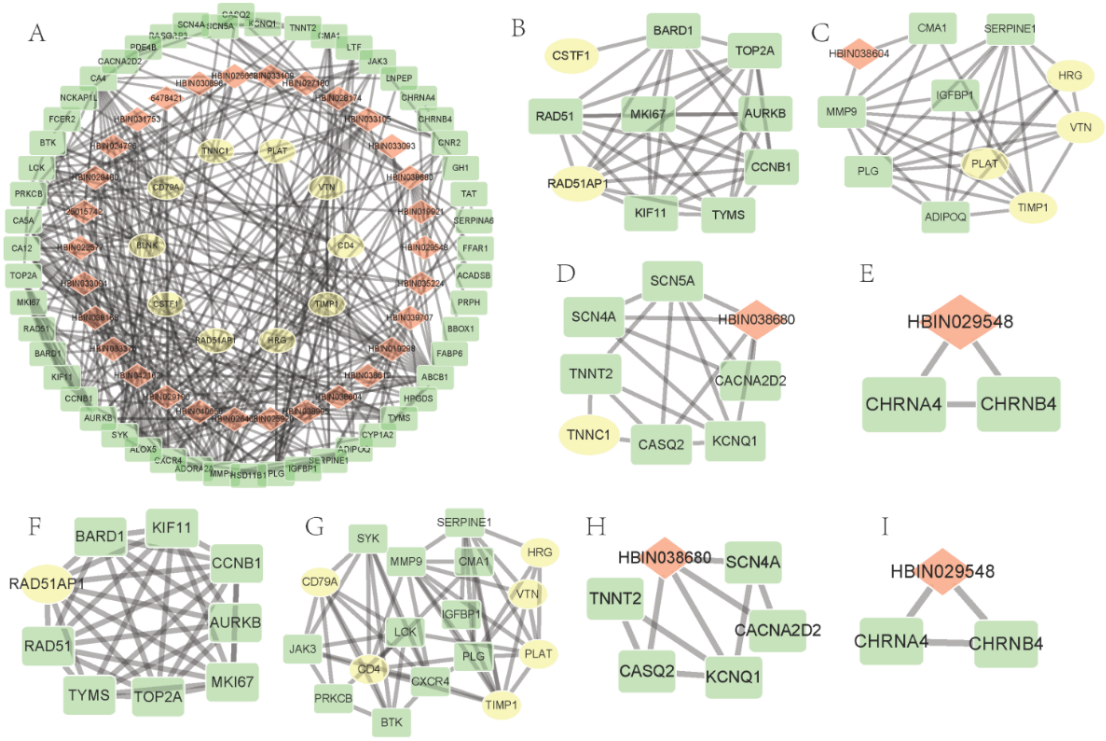

Figure 7. MCODE and ClusterONE analysis of the component-target network. A: The protein-protein interaction network of the intersecting targets, B–E: clusters 1–4, F–I: modules 1–4. Red boxes represent chemicals in SYGC, green boxes represent intersecting targets between SYGC and SOD DEGs, and yellow boxes represent interaction proteins in the STRING database.

3.7. Molecular docking validation

The present study examined the intersecting genes between MCODE and ClusterONE genes involved in the B cell receptor signaling pathway (AURKB, KIF11) and complement system (PLG). Each of the enriched components is docked with the three genes. The binding energy of ligands in

PDB structures was used for positive control (VX6 for AURKB: -8.8 kcal/mol, GCE for KIF11: -9.5 kcal/mol, XO3 for PLG: -7 kcal/mol). Glycycoumarin and licoflavonol exert lower score than VX4 ligand for AURKB target, indicating a strong binding activity. Rhamnocitrin shows a relative lower score compared to GCE ligand for KIF11 target, indicating a good binding activity. Echinatin, homobutein and licoflavonol present a relative lower score compared to XO3 ligand for PLG target, suggesting a good binding activity (Table 4).

Specifically, AURKB showed 12 interactions with glycycoumarin, including unfavorable donor-donor, Pi-sigma, Pi-alkyl and Alkyl, which were connected with GLU 161, LEU 83, ALA 157, VAL 91 and PHE 88 (Figure 8A). It showed 13 interactions with licoflavonol including carbon hydrogen bond, conventional hydrogen bond, unfavorable donor- donor, Pi-sigma, Pi-alkyl and Alkyl, which were connected with VAL 91, LYS 106, ALA 157, GLU 161 and GLY 160 (Figure 8B). KIF11 showed 8 interactions with rhamnocitrin, including conventional hydrogen bonds, Pi-sigma, Pi-alkyl and Pi-anion, which were connected with TRP 127, PRO 137, ALA 133, GLU 116 and ARG 119 (Figure 8C). PLG showed 6 interactions with echinatin including carbon hydrogen bond, conventional hydrogen bond, unfavorable donor- donor, Pi-cation, Pi-Pi stacked and Pi-Pi T-shaped, which were connected with TYR 72, ASP 55, ARG 71, TRP 62 and ARG 35 (Figure 8D). It showed 6 interactions with homobutein including carbon hydrogen bond, Pi-donor hydrogen bond, Pi-Pi stacked, Pi-Pi T-shaped, Pi-anion, Pi-alkyl and Pi-cation, which were connected with ARG 35, TRP 62, TYR 72, ASP 55 and ARG 71 (Figure 8E). It showed 9 interactions with licoflavonol including carbon hydrogen bond, Pi-Pi stacked, Pi-Pi T-shaped, Pi-anion, Alkyl and Pi-cation, which were connected with ASP 55, TRP 62, TYR 72, ASP 57 and ARG 35 (Figure 8F).

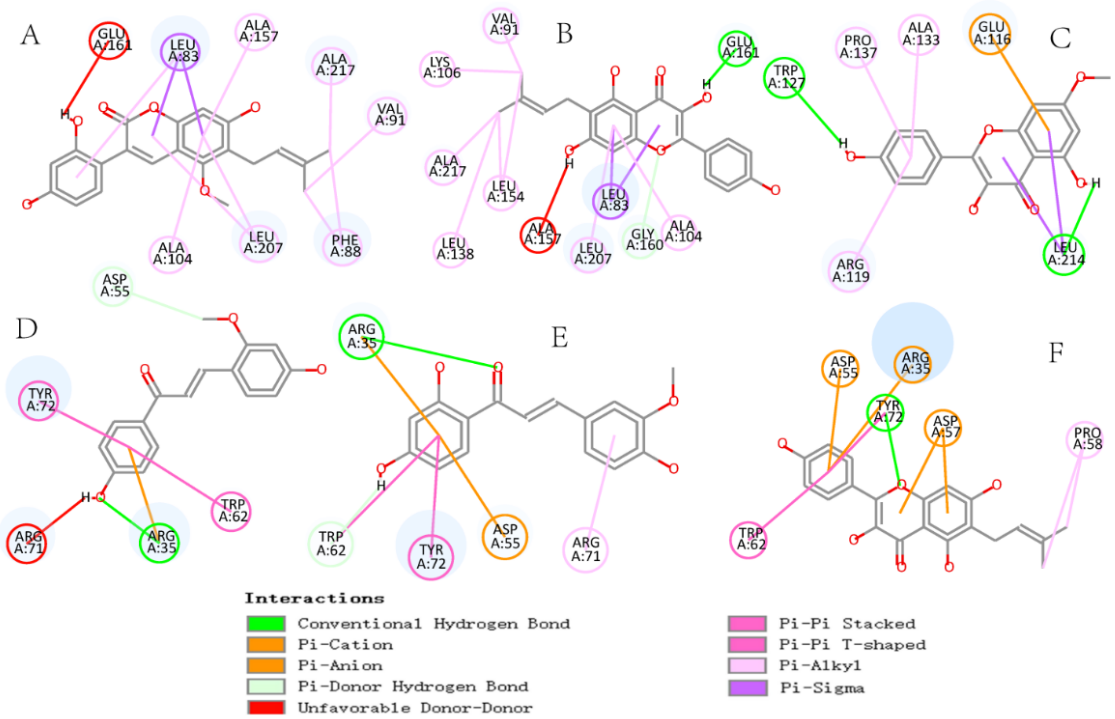

Figure 8. The docking model diagram of the active ingredient of the drug and the core target. A: AURKB-glycycoumarin, B: AURKB-licoflavonol, C: KIF1-rhamnocitrin, D: PLG-echinatin, E: PLG-homobutein, F: PLG-licoflavonol.

Table 4. The protein-ligand binding energy of molecular docking results (kcal/mol).

Ligand	Group	AURKB (4af3)	KIF11 (6hky)	PLG (4cik)
VX6_AURKB	control	-8.8	-	-
GCE_KIF11		-	-9.5	-
XO3_PLG		-	-	-7
Echinatin	SYGC	-8.4	-8.2	-6.4
Ethyl Gallate		-6.3	-6.1	-5.4
Glycycoumarin		-9.3	-7.9	-6.3
Hesperetin		-8.7	-8.6	-5.9
Homobutein		-8.2	-8.2	-6.4
Kaempferol		-8.8	-8.8	-6.3
Licoflavonol		-9.1	-7.5	-6.4
Methyl Gallate		-6.2	-6.2	-5.4
Palmitic Acid		-6.3	-6.2	-5
Rhamnocitrin		-8.3	-9	-6.3

3.8. Verifying of hub genes

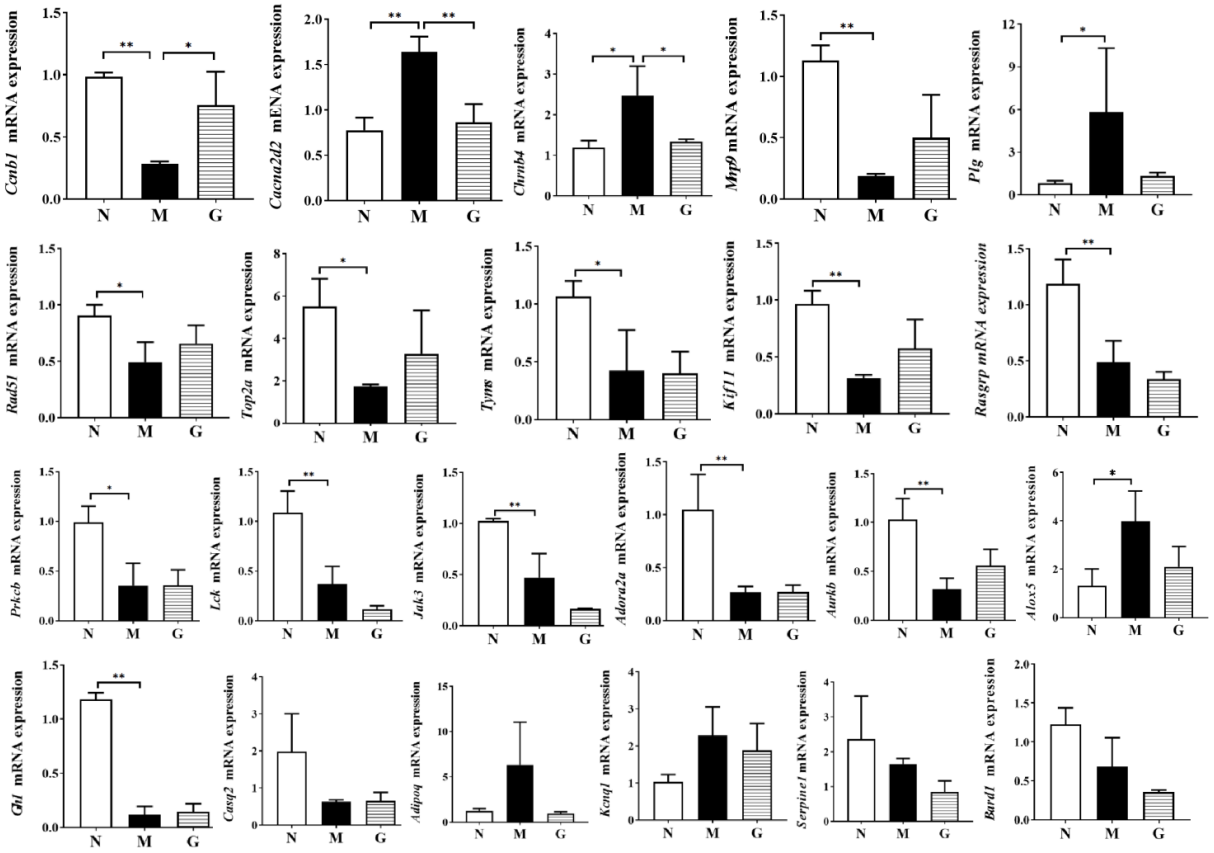

Figure 9. Validation of the mRNA expression levels of hub genes. *P < 0.05, **P < 0.01.

To verify the results of bioinformatics analysis, we obtained the top eight genes (*Prkcb, Alox5, Adora2a, Lck, Jak3, Rasgrp3, Adipoq* and *Gh1*) involved in the 52 gene-related signal pathways

and 14 intersecting genes (*Serpine1, Mmp9, Plg, Ccnb1, Cacna2d2, Rad51, Chrnb4, Aurkb, Top2a, Tyms, Kif11, Kcnq1, Casq2* and *Bard1*) among MCODE genes, ClusterONE genes and genes of significant enrichment pathways. We detected the mRNA expression levels of these genes by RT-qPCR in the Oddi sphincter tissues. Compared with the control group, the M group showed decreased expression of *Ccnb1, Mmp9, Rad51, Top2a, Tyms, Kif11, Rasgrp3, Prkcb, Lck, Jak3, Adora2a, Aurkb* and *Gh1* and increased expression of *Cacna2d2, Chrnb4, Alox5* and *Plg*. Moreover, the expression of *Ccnb1, Cacna2d2* and *Chrnb4* returned to normal after SYGC treatment (Figure 9).

4. Discussion

SOD is a key secondary pathological change in the context of gallbladder- and pancreas-related inflammatory diseases and seriously impacts patients' quality of life [18,19]. At present, the research on its pathogenesis and effective treatment are in the preliminary stages. TCM has been widely applied for the discovery of candidate drugs [20]. SYGC is used for the treatment of pain-related diseases with reducing muscle tension, relieving spasms and providing analgesia [21]. Moreover, paeoniflorin, an extract of Shaoyao, can relax the SO muscle via reducing calcium ion influx [22]. Isoliquiritigenin, a flavonoid from licorice, relaxed guinea-pig tracheal smooth muscle through the cGMP/PKG pathway [23]. Consistent with our clinical study [7], we also found that SYGC administration can repair the structure and ultrastructure of the SO in vivo with decreased inflammation infiltration and ring muscle disorders. However, the detailed regulatory mechanism of SYGC action against SOD requires further investigation.

Therefore, we used the systematic pharmacological method to discover the potential molecular mechanisms of SYGC on SOD. At first, a total of 649 DEGs were identified in SOD, which were mainly enriched in complement and coagulation cascades, B cell receptor signaling pathway, primary immunodeficiency and NF-kappa B signaling pathway. Recently, it was well established that immune disorders and inflammation played an important role in the occurrence and development of numerous diseases, including SOD [24–26]. The B cell receptor (BCR) signaling pathway was crucial for normal B cell development and adaptive immunity [27], and B cell-derived IgE may lead to smooth muscle contraction induced by the degranulation of mast cells [28]. NF-κB showed a key role in various biological processes, including inflammation, immune response, cell growth and survival and development [29–31]. NF-κB signaling impeded the recovery of skeletal muscle function after damage [32]. In addition, NF-kappaB activation served as a survival factor in B cell, which prevented cell apoptosis [33,34]. These results suggest that SOD may exert a dysfunction crosstalk between B cell receptor and NF-κB signaling pathway.

Then, does SYGC ameliorate SOD by regulating the B cell receptor signaling pathway? We first identified 32 candidate compounds using UHPLC-Q-Orbitrap-HRMS and network pharmacology analysis. Interestingly, these chemicals had an effect in the B cell receptor signaling pathway. Additionally, SYGC may improve SOD through multiple pathways including the complement system, Interleukin-4 and Interleukin-13 signaling and muscle contraction. Therefore, these results suggest that the B cell receptor signaling pathway may play a central role in these multiple pathways. For example, IL-4 and IL-13 exerted their signaling action by IL-4Rα/IL-13Rα complexes [35], and IL-4 was demonstrated to regulate B-cell receptor signaling in chronic lymphocytic leukemia [36]. The complement system, an essential contributor of innate immunity, was also important in regulating B cell responses at multiple stages of the peripheral response [37].

Combined with the effect of SYGC on muscle cramps [4,38], we speculate that SYGC improve SOD through relieving immune and inflammation dysfunction.

Additionally, we discovered three genes associated with the B cell receptor signaling pathway and complement system in the SYGC treatment of SOD, namely AURKB, KIF11 and PLG. Aurora kinase B (AURKB), which belongs to the mitotic protein kinase family, played a role in mitosis and the inflammatory pathway through of NF-κB transcription [39,40]. The plasminogen protein encoded by PLG can regulate skeletal muscle regeneration [41] and the resolution of inflammation through macrophage polarization and efferocytosis [42]. Moreover, the expression of these 3 genes returned to normal after SYGC treatment. These data imply that the three genes may play a critical role in the SYGC treatment of SOD.

Furthermore, glycycoumarin, licoflavonol, echinatin and homobutein exert good binding activity with the above three genes. It was reported that glycycoumarin can relax gastrointestinal smooth muscle tone [43] and inhibit tetanic contractions [38]. Echinatin and homobutein exerted favorable pharmacological effects on anti-inflammatory and anti-oxidant activity partly to NF-κB inhibition [44–46]. Collectively, these chemical components of SYGC provide the pharmacological basis for the immune and inflammation activities related to SOD.

5. Conclusions

In conclusion, the present study displayed that multi-ingredient therapeutics of SYGC regulated SOD development by multi-targets and multi-pathways. Future studies should be conducted to explore the involvement of these targets in the treatment of SOD with SYGC. In addition, more experiments are still needed to confirm our findings. Nevertheless, our research still provided some reasonable major mediators for the anti-SOD effects of SYGC, including four active compounds (glycycoumarin, licoflavonol, echinatin and homobutein), three targets (AURKB, KIF11 and PLG) and several pathways (B cell receptor signaling pathway, complement system and muscle contraction).

Acknowledgments

This work was supported by grants from the National Natural Science Foundation of China (No. 81904017).

Conflict of interest

The authors declare that the research was conducted in the absence of any commercial or financial relationships that could be construed as a potential conflict of interest.

References

1. K. R. K. K. Baig, C. M. Wilcox, Translational and clinical perspectives on sphincter of Oddi dysfunction, *Clin. Exp. Gastroenterol.*, **9** (2016), 191–195. https://doi.org/10.2147/CEG.S84018

2. P. B. Cotton, G. H. Elta, C. R. Carter, P. J. Pasricha, E. S. Corazziari, I. V. Rome, Gallbladder and Sphincter of Oddi disorders, *Gastroenterology*, **150** (2016), 1420–1429. https://doi.org/10.1053/j.gastro.2016.02.033
3. E. Afghani, S. K. Lo, P. S. Covington, B. D. Cash, S. J. Pandol, Sphincter of Oddi function and risk factors for dysfunction, *Front. Nutr.*, **4** (2017), 1. https://doi.org/10.3389/fnut.2017.00001
4. F. Hinoshita, Y. Ogura, Y. Suzuki, S. Hara, A. Yamada, N. Tanaka, et al., Effect of orally administered shao-yao-gan-cao-tang (Shakuyaku-kanzo-to) on muscle cramps in maintenance hemodialysis patients: A preliminary study, *Am. J. Chin. Med.*, **31** (2003), 445–453. https://doi.org/10.1142/S0192415X03001144
5. T. H. Wu, L. C. Chen, L. L. Yang, Hypouricemic effect and regulatory effects on autonomic function of Shao-Yao Gan-Cao Tang, a Chinese herbal prescription, in asymptomatic hyperuricemic vegetarians, *Rheumatol. Int.*, **28** (2007), 27–31. https://doi.org/10.1007/s00296-007-0385-7
6. H. Fujinami, S. Kajiura, J. Nishikawa, T. Ando, T. Sugiyama, The influence of duodenally-delivered Shakuyakukanzoto (Shao Yao Gan Cao Tang) on duodenal peristalsis during endoscopic retrograde cholangiopancreatography: A randomised controlled trial, *Chin. Med.*, **12** (2017), 3. https://doi.org/10.1186/s13020-016-0125-6
7. M. Chen, F. Li, X. J. Li, Y. P. Hu, B. Gong, X. W. Zhang, et al., Clinical study on the treatment of sphincter of Oddi dysfunction type II with Shaoyao Gancao decoction, *J. Guangzhou Univ. Tradit. Chin. Med.*, **38** (2021), 681–686.
8. J. Chen, Z. Q. Liang, C. Hu, Y. Gao, Y. K. Wang, J. W. Yang, et al., Protection against peripheral artery disease injury by Ruan Jian Qing Mai formula via metabolic programming, *Biotechnol. Appl. Biochem.*, **68** (2021), 366–380. https://doi.org/10.1002/bab.1934
9. J. Chen, Y. K. Wang, Y. Gao, L. S. Hu, J. W. Yang, J. R. Wang, et al., Protection against COVID-19 injury by qingfei paidu decoction via anti-viral, anti-inflammatory activity and metabolic programming, *Biomed. Pharmacother.*, **129** (2020), 110281. https://doi.org/10.1016/j.biopha.2020.110281
10. M. Yang, J. Sun, Z. Lu, G. Chen, S. Guan, X. Liu, et al., Phytochemical analysis of traditional Chinese medicine using liquid chromatography coupled with mass spectrometry, *J. Chromatogr. A*, **1216** (2009), 2045–2062. https://doi.org/10.1016/j.chroma.2008.08.097
11. A. Daina, O. Michielin, V. Zoete, SwissADME: A free web tool to evaluate pharmacokinetics, drug-likeness and medicinal chemistry friendliness of small molecules, *Sci. Rep.*, **7** (2017), 42717. https://doi.org/10.1038/srep42717
12. S. Fang, L. Dong, L. Liu, J. Guo, L. Zhao, J. Zhang, et al., HERB: A high-throughput experiment- and reference-guided database of traditional Chinese medicine, *Nucleic Acids Res.*, **49** (2021), D1197–D1206. https://doi.org/10.1093/nar/gkaa1063
13. A. Daina, O. Michielin, V. Zoete, SwissTargetPrediction: updated data and new features for efficient prediction of protein targets of small molecules, *Nucleic Acids Res.*, **47** (2019), W357–W364. https://doi.org/10.1093/nar/gkz382
14. Z. Liu, F. Guo, Y. Wang, C. Li, X. Zhang, H. Li, et al., BATMAN-TCM: A bioinformatics analysis tool for molecular mechanism of traditional Chinese medicine, *Sci. Rep.*, **6** (2016), 21146. https://doi.org/10.1038/srep21146

15. Y. Zhou, B. Zhou, L. Pache, M. Chang, A. H. Khodabakhshi, O. Tanaseichuk, et al., Metascape provides a biologist-oriented resource for the analysis of systems-level datasets, *Nat. Commun.*, **10** (2019), 1523. https://doi.org/10.1038/s41467-019-09234-6
16. G. Su, J. H. Morris, B. Demchak, G. D. Bader, Biological network exploration with Cytoscape 3, *Curr. Protoc. Bioinf.*, **47** (2014), 1–24. https://doi.org/10.1002/0471250953.bi0813s47
17. T. Nepusz, H. Yu, A. Paccanaro, Detecting overlapping protein complexes in protein-protein interaction networks, *Nat. Methods*, **9** (2012), 471–472. https://doi.org/10.1038/nmeth.1938
18. W. D. Leung, S. Sherman, Endoscopic approach to the patient with motility disorders of the bile duct and sphincter of Oddi, *Gastrointest. Endosc. Clin.*, **23** (2013), 405–434. https://doi.org/10.1016/j.giec.2012.12.006
19. G. Y. Zhu, D. D. Jia, Y. Yang, Y. Miao, C. Wang, C. M. Wang, The effect of Shaoyao Gancao decoction on sphincter of Oddi dysfunction in hypercholesterolemic rabbits via protecting the enteric nervous system-interstitial cells of cajal-smooth muscle cells network, *J. Inflamm. Res.*, **14** (2021), 4615–4628. https://doi.org/10.2147/JIR.S326416
20. J. Park, D. Jeong, M. Song, B. Kim, Recent advances in anti-metastatic approaches of herbal medicines in 5 major cancers: from traditional medicine to modern drug discovery, *Antioxidants*, **10** (2021), 527. https://doi.org/10.3390/antiox10040527
21. Y. Y. Shao, Y. T. Guo, J. P. Gao, J. J. Liu, Z. P. Chang, X. J. Feng, et al., Shaoyao-Gancao decoction relieves visceral hyperalgesia in TNBS-induced postinflammatory irritable bowel syndrome via inactivating transient receptor potential vanilloid type 1 and reducing serotonin synthesis, *Evid. Based Complement. Alternat. Med.*, **2020** (2020), 7830280. https://doi.org/10.1155/2020/7830280
22. F. Wang, Y. Yang, X. Ji, X. Tao, Y. Wang, C. Wang, Effects of Paeoniflorin on the activity of muscle strips, intracellular calcium ion concentration and Ltype voltagesensitive calcium ion channels in the sphincter of Oddi of hypercholesterolemic rabbits, *Mol. Med. Rep.*, **19** (2019), 5185–5194. https://doi.org/10.3892/mmr.2019.10183
23. B. Liu, J. Yang, Q. Wen, Y. Li, Isoliquiritigenin, a flavonoid from licorice, relaxes guinea-pig tracheal smooth muscle in vitro and in vivo: role of cGMP/PKG pathway, *Eur. J. Pharmacol.*, **587** (2008), 257–266. https://doi.org/10.1016/j.ejphar.2008.03.015
24. M. A. Ballal, P. A. Sanford, Physiology of the sphincter of Oddi—the present and the future?—Part 1, *Saudi J. Gastroenterol.*, **6** (2000), 129–146. https://www.saudijgastro.com/text.asp?2000/6/3/129/33475
25. Y. Wang, H. Chang, Y. Zhang, K. Wang, H. Zhang, X. Yan, et al., Endoscopic endoclip papilloplasty preserves sphincter of oddi function, *Eur. J. Clin. Invest.*, **51** (2021), e13408. https://doi.org/10.1111/eci.13408
26. H. Sato, T. Kodama, J. Takaaki, Y. Tatsumi, T. Maeda, S. Fujita, et al., Endoscopic papillary balloon dilatation may preserve sphincter of Oddi function after common bile duct stone management: evaluation from the viewpoint of endoscopic manometry, *Gut*, **41** (1997), 541–544. https://doi.org/10.1136/gut.41.4.541
27. J. A. Burger, A. Wiestner, Targeting B cell receptor signalling in cancer: preclinical and clinical advances, *Nat. Rev. Cancer*, **18** (2018), 148–167. https://doi.org/10.1038/nrc.2017.121
28. R. K. Martin, S. R. Damle, Y. A. Valentine, M. P. Zellner, B. N. James, J. C. Lownik, et al., B1 cell IgE impedes mast cell-mediated enhancement of parasite expulsion through B2 IgE blockade, *Cell Rep.*, **22** (2018), 1824–1834. https://doi.org/10.1016/j.celrep.2018.01.048

29. S. Vallabhapurapu, M. Karin, Regulation and function of NF-kappaB transcription factors in the immune system, *Annu. Rev. Immunol.*, **27** (2009), 693–733. https://doi.org/10.1146/annurev.immunol.021908.132641
30. M. S. Hayden, S. Ghosh, Shared principles in NF-kappaB signaling, *Cell*, **132** (2008), 344–362. https://doi.org/10.1016/j.cell.2008.01.020
31. S. C. Sun, Non-canonical NF-kappaB signaling pathway, *Cell Res.*, **21** (2011), 71–85. https://doi.org/10.1038/cr.2010.177
32. T. S. O. Jameson, G. F. Pavis, M. L. Dirks, B. P. Lee, D. R. Abdelrahman, A. J. Murton, et al., Reducing NF-kappaB signaling nutritionally is associated with expedited recovery of skeletal muscle function after damage, *J. Clin. Endocrinol. Metab.*, **106** (2021), 2057–2076. https://doi.org/10.1210/clinem/dgab106
33. J. Choi, J. D. Phelan, G. W. Wright, B. Haupl, D. W. Huang, A. L. Shaffer, et al., Regulation of B cell receptor-dependent NF-kappaB signaling by the tumor suppressor KLHL14, *Proc. Natl. Acad. Sci.*, **117** (2020), 6092–6102. https://doi.org/10.1073/pnas.1921187117
34. C. I. E. Smith, J. A. Burger, Resistance mutations to BTK inhibitors originate from the NF-kappaB but not from the PI3K-RAS-MAPK arm of the B cell receptor signaling pathway, *Front. Immunol.*, **12** (2021), 689472. https://doi.org/10.3389/fimmu.2021.689472
35. R. Hurdayal, F. Brombacher, Interleukin-4 receptor alpha: From innate to adaptive immunity in murine models of cutaneous leishmaniasis, *Front. Immunol.*, **8** (2017), 1354. https://doi.org/10.3389/fimmu.2017.01354
36. B. Guo, L. Zhang, N. Chiorazzi, T. L. Rothstein, IL-4 rescues surface IgM expression in chronic lymphocytic leukemia, *Blood*, **128** (2016), 553–562. https://doi.org/10.1182/blood-2015-11-682997
37. S. Freeley, C. Kemper, G. L. Friec, The "ins and outs" of complement-driven immune responses, *Immunol. Rev.*, **274** (2016), 16–32. https://doi.org/10.1111/imr.12472
38. K. K. Lee, Y. Omiya, M. Yuzurihara, Y. Kase, H. Kobayashi, Antispasmodic effect of shakuyakukanzoto extract on experimental muscle cramps in vivo: Role of the active constituents of Glycyrrhizae radix, *J. Ethnopharmacol.*, **145** (2013), 286–293. https://doi.org/10.1016/j.jep.2012.11.005
39. A. Madejon, J. Sheldon, I. Francisco-Recuero, C. Perales, M. Dominguez-Beato, M. Lasa, et al., Hepatitis C virus-mediated Aurora B kinase inhibition modulates inflammatory pathway and viral infectivity, *J. Hepatol.*, **63** (2015), 312–319. https://doi.org/10.1016/j.jhep.2015.02.036
40. Z. Wang, Z. Yu, G. H. Wang, Y. M. Zhou, J. P. Deng, Y. Feng, et al., AURKB promotes the metastasis of gastric cancer, possibly by inducing EMT, *Cancer Manage. Res.*, **12** (2020), 6947–6958. https://doi.org/10.2147/CMAR.S254250
41. M. Suelves, R. Lopez-Alemany, F. Lluis, G. Aniorte, E. Serrano, M. Parra, et al., Plasmin activity is required for myogenesis in vitro and skeletal muscle regeneration in vivo, *Blood*, **99** (2002), 2835–2844. https://doi.org/10.1182/blood.v99.8.2835
42. J. P. Vago, M. A. Sugimoto, K. M. Lima, G. L. Negreiros-Lima, N. Baik, M. M. Teixeira, et al., Plasminogen and the plasminogen receptor, Plg-RKT, regulate macrophage phenotypic, and functional changes, *Front. Immunol.*, **10** (2019), 1458. https://doi.org/10.3389/fimmu.2019.01458

43. Y. Sato, T. Akao, J. X. He, H. Nojima, Y. Kuraishi, T. Morota, et al., Glycycoumarin from Glycyrrhizae Radix acts as a potent antispasmodic through inhibition of phosphodiesterase 3, *J. Ethnopharmacol.*, **105** (2006), 409–414. https://doi.org/10.1016/j.jep.2005.11.017
44. G. Xu, S. Fu, X. Zhan, Z. Wang, P. Zhang, W. Shi, et al., Echinatin effectively protects against NLRP3 inflammasome-driven diseases by targeting HSP90, *JCI Insight*, **6** (2021), e134601. https://doi.org/10.1172/jci.insight.134601
45. K. Yonekura-Sakakibara, Y. Higashi, R. Nakabayashi, The origin and evolution of plant flavonoid metabolism, *Front. Plant. Sci.*, **10** (2019), 943. https://doi.org/10.3389/fpls.2019.00943
46. B. Orlikova, M. Schnekenburger, M. Zloh, F. Golais, M. Diederich, D. Tasdemir, Natural chalcones as dual inhibitors of HDACs and NF-kappaB, *Oncol. Rep.*, **28** (2012), 797–805. https://doi.org/10.3892/or.2012.1870

AIMS Press